International Journal of Civil Engineering and Technology (IJCIET)
Volume 7, Issue 1, Jan-Feb 2016, pp. 128-139, Article ID: IJCIET_07_01_011
Available online at
http://www.iaeme.com/IJCIET/issues.asp?JType=IJCIET&VType=7&IType=1
Journal Impact Factor (2016): 9.7820 (Calculated by GISI) www.jifactor.com
ISSN Print: 0976-6308 and ISSN Online: 0976-6316

FINITE ELEMENT THERMAL ANALYSIS OF DEEP BOX-GIRDERS

Sallal R. Abid
Assistant Professor, Civil Engineering Department, College of Engineering, Wasit University, Kut, Iraq

Salih Alrebeh
Engineering Projects Unit, Thiqar University, Nasiriyah, Iraq

Nildem Tayşi
Assistant Professor, Civil Engineering Department, College of Engineering, Gaziantep University, Gaziantep, Turkey

Mustafa Özakça
Professor, Civil Engineering Department, College of Engineering, Gaziantep University, Gaziantep, Turkey

ABSTRACT

A three-dimensional thermal analysis using the finite element method was conducted in this research to evaluate the heat conduction in deep concrete box-girder bridges considering the temperature change of air, the thermal radiation from the sun and the speed of the wind. The current finite element analysis has predicted the concrete temperatures effectively with temperature errors ranged between 0.1 ^{o}C and 1.7 ^{o}C. The proposed finite element model was then used to evaluate the distribution of temperature in deep concrete box-girders considering the weather conditions of Gaziantep, Turkey. The weather data including solar radiation, air temperature and wind speed for a hot summer day were recorded from a specially installed weather station in the campus of the University of Gaziantep. The results showed that the AASHTO's gradient model was almost identical with the predicted temperature gradients at the top and the bottom surfaces and along the clear depth of the webs. However, the behavior along the top 1 m was different.

Key words: Air Temperature, Deep Box-Girder, Solar Radiation and Temperature Gradient

Cite this Article: Sallal R. Abid, Salih Alrebeh, Nildem Tayşi and Mustafa Özakça. Finite Element Thermal Analysis of Deep Box-Girders. *International Journal of Civil Engineering and Technology*, **7**(1), 2016, pp. 128-139.
http://www.iaeme.com/IJCIET/issues.asp?JType=IJCIET&VType=7&IType=1

1. INTRODUCTION

Many types of structures are constructed in open environments, thus suffer a continuous exposure to the fluctuation of climate. Bridges are among the structures where the diurnal and seasonal variations in solar radiation and air temperature affect the serviceability and may cause serious cracks and deflections [1-5], which influence the live span of the bridge [6]. Many of the leading researches that were carried out during the period extended from 1970 to 1990 [7-9] were the basis of the thermal actions provisions of respected bridge design codes.

Most of the existing bridge design codes around the world, take into consideration the temperature gradients that occur along the depth of the superstructure. The temperature gradient models suggested by the design codes are generally linear, multi-linear or nonlinear, which consider both the heating (positive) temperature gradients and the cooling (negative) temperature gradients. The positive gradient occurs after the continuous heating of the top surface during the hot hours of the day, causing a significant rise in the temperature there compared to the temperature of the interior sections, while the negative gradient occurs within the early morning hours after long cooling phase at the top surface, which leads to a reverse temperature differential.

AASHTO [10] specifies a bilinear gradient model for both the positive and the negative temperature gradients. Four climate regions are categorized by AASHTO according to the maximum solar intensity in USA and are defined from zone 1 to zone 4. The bilinear model consists of three temperatures gradients. The maximum at the top surface (T1), followed by a linear decrease to the temperature gradient T2, which is located 0.1 m below the top surface. The gradient decreases from T2 to zero at a depth of 0.4 m for most cases. At the lower surface of the bottom slab, a temperature gradient T3 is suggested, which varies linearly along the lower 0.2 m of the superstructure.

In this paper, the influences of the daily change in the ambient air temperature and the variation of the intensity of solar thermal radiation on the thermal budget in deep box-girder bridges were studied using a three-dimensional finite element modeling of an existing bridge. The temperature distributions along and across the slabs and the webs of the girder and the vertical temperature gradients were investigated for the climate of Gaziantep, Turkey. In addition, a comparison was made between the predicted maximum temperature gradient and the design gradient of the AASHTO bridge design specifications.

2. HEAT TRANSFER IN BOX-GIRDERS

The thermal changes of heat and temperature through the different parts of the bridge cross section and along its span, which is a three-dimensional heat flow problem, is controlled by the Fourier heat transfer equation [11],

$$\rho C \frac{\partial T}{\partial t} = k\left(\frac{\partial^2 T}{\partial x^2} + \frac{\partial^2 T}{\partial y^2} + \frac{\partial^2 T}{\partial z^2}\right) + Q \qquad (1)$$

where ρ, C and k are the concrete density, specific heat and thermal conductivity, respectively, while Q is the heat generated by cement hydration. The temperature T is the main variable, which varies with x, y, and z.

The boundary conditions on the girder's surfaces are described by [11],

$$k\left(\frac{\partial T}{\partial x}n_x + \frac{\partial T}{\partial y}n_y + \frac{\partial T}{\partial z}n_z\right) + q = 0 \quad (2)$$

where q is the heat exchange between the exposed surfaces and the surrounding environment per unit area, while n_x, n_y, n_z are the direction cosines of the unit vectors normal to the surfaces in the directions x, y and z.

$$q = h_c(T_s - T_a) + \alpha I + \alpha\beta I\left(\frac{1-\cos\theta}{2}\right) + \epsilon\sigma(T_s^4 - T_a^4) \quad (3)$$

The first term is the surface convection with the surrounding air, where h_c is the convection coefficient of the surface, T_s is the surface temperature and T_a is the temperature of the ambient air. The second term is the solar radiation absorbed by the exposed surfaces, while the third term describes the reflected radiation from the ground and other surroundings. Where, α is the absorptivity of the surfaces, I is the global solar radiation on a horizontal surface, β is the reflection coefficient of the ground, and θ is the tilt angle of surface. Finally, the last term represents the thermal radiosity of the exposed surfaces to the atmosphere, where ϵ is the emissivity of the surface and σ is the Stefan-Boltzmann constant. To solve Eq. (1) and to apply the boundary loads that described in Eq. (3), the finite element package COMSOL Multiphysics [12] was used.

Table 1 Material and thermal loads values

k (W/m K)	**C J/Kg K**	**ϵ**	**α**
1.7	1000	0.9	0.5
Maximum T_a (℃)	**Minimum T_a (℃)**	**Wind Speed**	**Albedo**
28.6	21.6	29.5	0.1

3. VERIFICATION OF THE FINITE ELEMENT ANALYSIS

The current finite element model was compared with experimental results from a box-girder bridge with variable cross-section along the span, which was constructed in New Brunswick, Canada [13]. The comparison was conducted for the deepest cross-section in August 9, 1998 at 3:00 PM. The material thermal properties were assumed equal to those considered by Sveinson [13], which are shown in Table 1, which also lists the air temperature range, wind speed and the used albedo coefficient. Figure 1(a) shows the compared section, in which the detailed cross-sectional dimensions and the sections along which the thermocouples were installed are illustrated.

As shown in Figure 1(a), three sets of thermocouples were installed across the top slab (TS1, TS2 and TS3), one set was installed across the bottom slab (BS1) and four sets of thermocouples were installed across the two webs (W1, W2, W3 and W4). Sections TS1, TS2 and BS1 have five thermocouples each, while the rest groups have three thermocouples each.

The Average Absolute Error (AAE) and the Maximum Absolute Error (MAE) for the eight sections are listed in Table 2. Both the AAE and MAE and for the eight groups were noticeably small, where the AAE for the eight groups ranged between approximately 0.1 ℃ and 1.1 ℃, while MAE ranged from approximately 0.2 ℃ to approximately 1.7 ℃. The values of AAE and MAE show that the predicted temperatures in the current study matched well with the compared field temperatures. The finite element three-dimensional temperature distribution in the girder segment at

3:00 PM is shown in Figure 1(b). Figures 2 to 4 show the degree of agreement between the predicted temperatures and those recorded in the field along BS1, TS1 and along W1 and W2 sections, respectively. The figures clearly illustrate the good agreement between the predicted and the experimental results and confirm the ability of the current finite element model to analyze the box-girder with all boundary loads efficiently. In addition to the presented verification, this models was verified in previous works with an experimental box-girder [14, 15] and with other types of concrete girders [16].

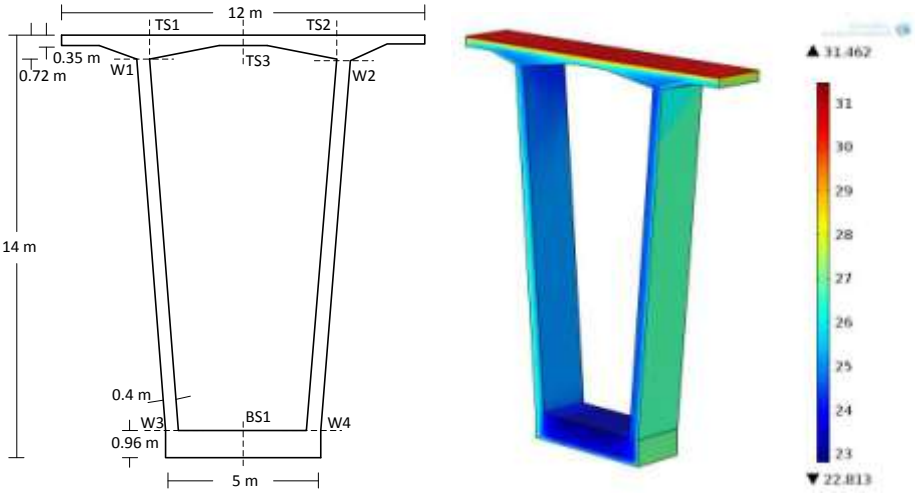

(a) Cross-section (b) Predicted temperature distribution at 3:00 PM

Figure 1 The deep box-girder, (a) the cross-section of the tested box-girder [13] and (b) the three-dimensional finite element temperature distribution at 3:00 PM

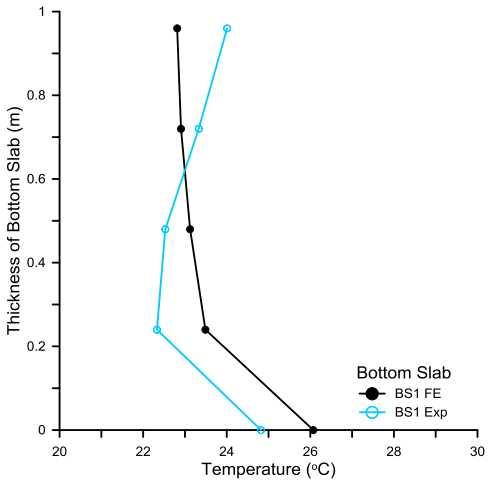

Figure 2 Comparison of the finite element predicted and the field temperatures along BS1 section

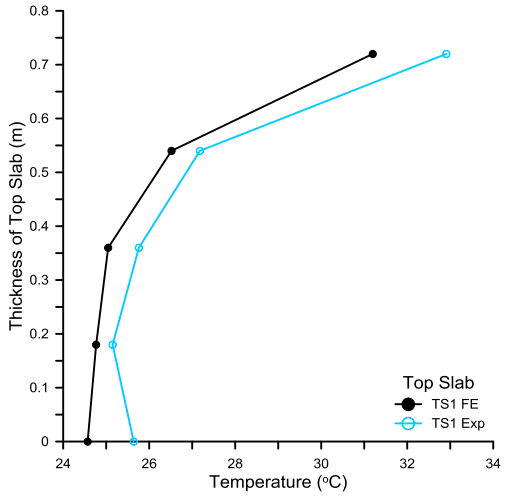

Figure 3 Comparison of the finite element predicted and the field temperatures along TS1 section

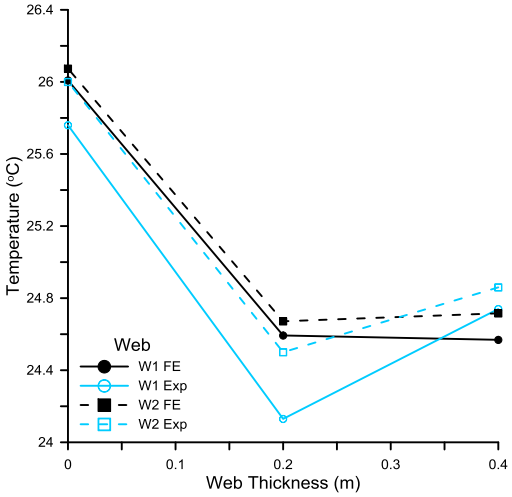

Figure 4 Comparison of the finite element predicted and the field temperatures along W1 and W2 sections

4. TEMPERATURE GRADIENTS IN GAZIANTEP

To study the temperature distributions and the resulting gradients in deep box-girder bridges in Gaziantep, air temperature, solar radiation and wind speed records were collected from a weather station installed in the campus of the University of Gaziantep. The June 2 was found to have the highest hourly global solar radiation record along the summer of 2013 which was 1200 W/m^2 [17]. The maximum and minimum air temperatures in the same day were 31.5 and 12.1 ℃, respectively. The wind speed on June 2 ranged from 0 to 1.9 m/s with an average of 0.7 m/s. To simplify the numerical study, the cross-section of the top slab was simplified to be prismatic with 0.7 m thickness. To maximize the vertical temperature gradient along the webs, the longitudinal axis of the bridge was considered along the east-west direction so that the webs face the south and the north.

Figure 5(a) shows the vertical temperature distribution along the 14.0 m depth of the south web of the box-girder at different time steps [18]. The temperature distribution at 6:00 AM represents those of the early morning hours, at which the top surface is colder than the lower interior sections. The temperature of the top surface at

6:00 AM was 26.6 ℃, while the temperature in an interior point located 0.3 m below the top surface was about 30 ℃ as shown in Figure 5(a) and clearly illustrated in Figure 5(b). After the continuous heating of the top surface during the midday hours, which are associated with high solar radiation fluxes, the surface reached its maximum temperature between 1:00 PM and 2:00 PM making a high differential from the temperature of the lower layers along the top slab and the web as shown in Figure 5(a). It is shown in Figures 5(a) and 5(b) that the temperature of the top surface at 2:00 PM was more than 52 ℃, while the temperature at 1.0 m below was less than 25 ℃. After the sunset, the temperature of the top surface decreased gradually while the temperature of the interior points of the top slab stilled relatively higher as illustrated in the temperature distribution at 8:00 PM. This decrease continued during the night hours and early morning hours because of the effect of the surface convection cooling and the surface long-wave radiation to atmosphere, reaching the minimum surface temperature before the sunrise as shown in the temperature distribution at 6:00 AM as illustrated in Figures 5(a) and 5(b).

A general notice, which can be recognized for each of the three time steps, is that the temperature was almost constant along the clear depth of the web, which is extended from the bottom surface of the top slab to the top surface of the bottom slab as shown in Figure 5(a).

As shown in Figure 5(a), the temperature distribution across the bottom slab differs from a time step to another. This variation is more clearly illustrated in Figure 6(a). As shown in Figure 6(a), the bottom surface of the bottom slab suffered higher temperatures than the inside concrete points at 2:00 PM. This can be attributed to the effect of the diffused solar radiation, the hot air temperature and the reflected radiation from the ground and other surroundings. The temperature at the bottom surface along the south web was 26.6 ℃ at 2:00 PM, while at 0.2 m deeper in the concrete of the bottom slab, the temperature decreased to 23.8 ℃. Beyond the hot hours of the day, the solar radiation reduced gradually and the air temperature decreased leading to the starting of the cooling process on the bottom surface as shown in the temperature distribution at 8:00 PM in Figure 6(a). The convection and the re-radiation surface cooling continued until a reverse temperature distribution took place, which reached its maximum before sunrise as shown in the temperature distribution at 6:00 AM in Figure 6(a), in which the surface temperature was approximately 19 ℃, while it was approximately 23 ℃ at depths deeper than 0.2 m from the bottom surface.

Figure 6(b) shows the temperature distribution across the section WS, which was taken across the thickness of the south web at the mid-depth of the web. The figure shows that the exterior surface temperature was higher than that of the interior surface at 2:00 PM by 6.5 ℃, while it was lower than that of the interior surface by approximately 5 ℃ at 6:00 AM. As shown in Figure 6(b), at 8:00 PM, the temperature difference between the exterior surface and the interior surface is minimal, where the starting of the cooling phase set the surface temperature down.

Figures 7(a) and 7(b) show the temperature distributions at the three time steps along the centerline of the 12 m width of the top slab and the 5 m width of the bottom slab, respectively. It is shown in Figure 7(a) that for each of the three time steps, the temperature was approximately the same along the central width of the slab, while sharp temperature deviation occurred along the southern cantilever slab and lower temperature deviation occurred along the northern cantilever slab. At 6:00 AM, the temperature decreased from approximately 30 ℃ at 0.5 m away from the edge to

approximately 21.5 ℃ at the southern edge, while the difference was only 3 ℃ along the northern edge as shown in Figure 7(a). Similar results were observed at 8:00 PM but with lower temperature differentials. At 2:00 PM, the temperature of the southern edge was higher by about 4.5 ℃ as shown in Figure 7(a).

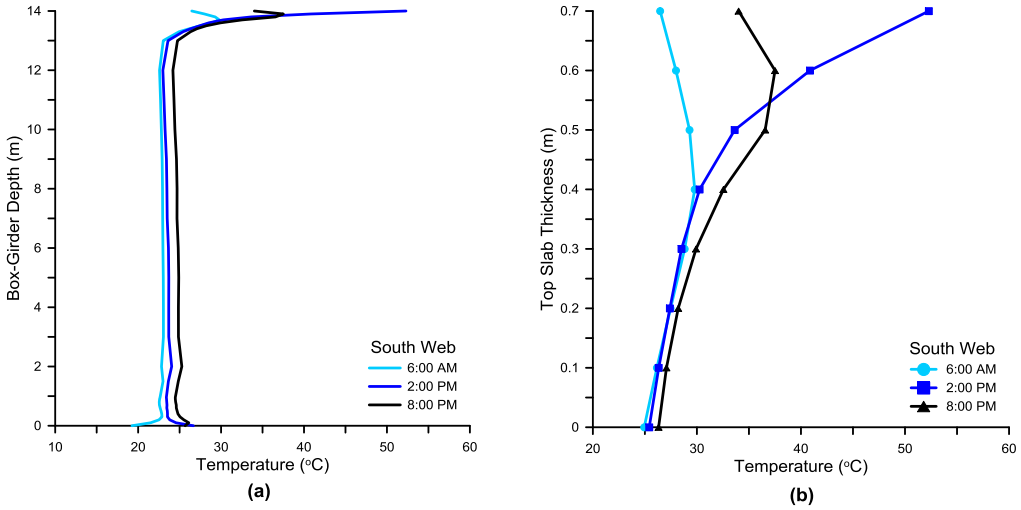

Figure 5 Temperature distributions along the centerline of the south web at different time steps (a) along the depth of girder and (b) across the thickness of the top slab

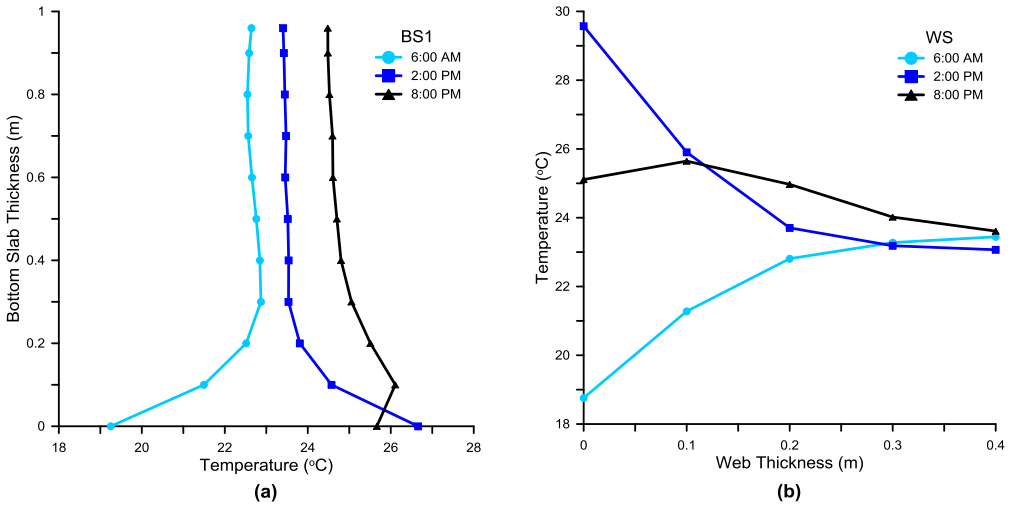

Figure 6 Temperature distributions at different time steps (a) across the thickness of the bottom slab (b) across the thickness of the south web

During summer, the sun rises from the northeast and sets at the northwest striking with low angles and lower solar radiations. While during the hot hours, which extended from approximately 10:00 AM to approximately 4:00 PM, sunrays strike the bridge from the south with higher altitudes and higher solar radiation intensity. This explains why the maximum temperature gradients occur at the southern surfaces [19]. This explanation can be obviously observed in the temperature distribution along the bottom slab at 6:00 AM, which is shown in Figure 7(b). At the northern surface, the edge was heated up after short time from sunrise due to the low altitude sunrays concentrated there, while the completely shaded southern edge continued cooling down. Thus, the temperature gradient was positive (heating) along the northern edge, while it was negative (cooling) along the southern edge. The temperature distribution

at 8:00 PM, which was close to the sunset, also confirms that the low altitude striking of sunrays near the sunrise and sunset hours increased the temperature of the northern surface of the bottom slab causing higher temperature gradients than at the southern surfaces as shown in Figure 7(b).

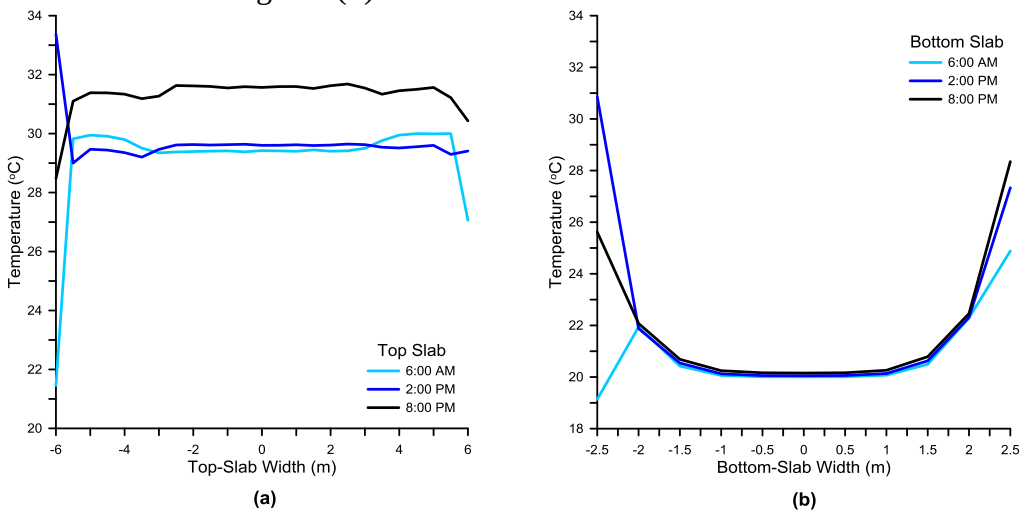

Figure 7 Temperature distributions at different time steps (a) along the top slab (b) along the bottom slab

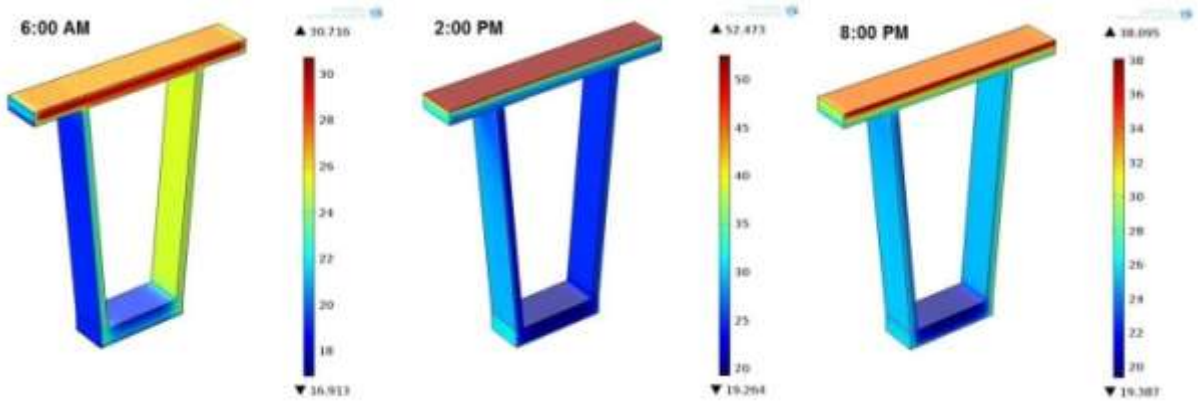

Figure 8 The three-dimensional temperature distributions in the box-girder segment at 6:00 AM, 2:00 PM and 8:00 PM

As shown in the temperature distribution at 2:00 PM, the temperature gradient occurred along the bottom slab was much higher that along the top slab at the same time step. The temperature gradient was about 11 ℃ at the southern surface of the bottom slab, while it was only about 4.5 ℃ at the southern surface of the top slab. Figure 8 shows the three-dimensional temperature distributions in the box-girder segment at 6:00 AM, 2:00 PM and 8:00 PM.

5. VERTICAL TEMPERATURE GRADIENTS

Figure 9 shows the distribution of the maximum temperature gradient along the whole 14 m depth of the girder at the time steps of maximum positive and negative gradients. The maximum negative temperature gradient occurred at 5:40 AM along the south web, while it occurred at 5:20 AM along the north web as shown in Figures 9(a) and 9(b), respectively. The effect of the top slab's thickness is clear in Figures 9(a) and (b), in which it is shown that the gradient occurred within the thickness of the top slab, while the temperature was almost constant within the clear height of the

webs. The thickness of the top slab is 0.7 m, while the thermal conductivity of concrete is weak (1.7 $W/m\,K$) so that it is not adequate to conduct the surface's low temperatures to the lower surface or even beyond the mid-thickness of the slab within the night cooling hours. Thus, the deeper points of the top slab kept their hot temperatures even after the long cooling hours, causing a reversed temperature gradient within the thickness of the slab. The maximum surface negative temperature gradients along the south and the north webs were 10.7 ℃ and 10.8 ℃, respectively.

The temperature along the clear depth of the web was approximately 23 ℃ for the south web and 25 ℃ for the north web at 5:40 AM and 5:20 AM, respectively. Along the thickness of the bottom slab, the temperature gradients at the same time steps were approximately 4 ℃ and 5 ℃ for the south and the north webs, respectively.

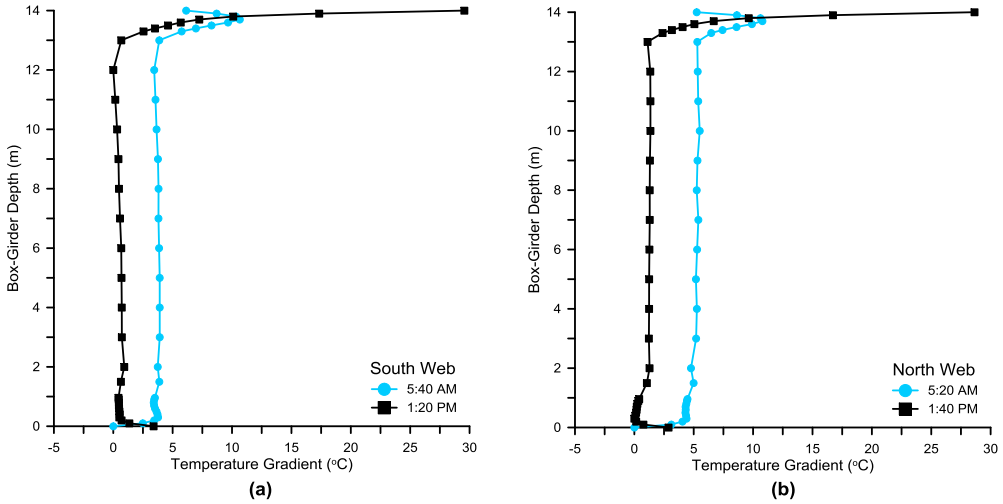

Figure 9 Vertical temperature gradients along the depth of the girder at different time steps (a) along the centerline of the south web and (b) along the centerline of the north web

Three distinguishable regions can be recognized in the positive gradients along the depth of the girder. First, a sharp nonlinear temperature decrease within the thickness of the top slab or at most within the top 1 m, followed by a region of a semi-constant temperature, which mostly extends along the clear depth of web in addition to the top 0.7 m of the bottom slab. The third region extends along the bottom 0.2 m of the bottom slab, within which the temperature shows a limited semi-linear increase up to a maximum at the bottom surface of the bottom slab. The three regions are obvious in Figures 9(a) and 9(b).

The maximum positive temperature gradients occurred between 1:20 PM and 1:40 PM. The maximum surface temperature gradients along the south and the north webs were 29.6 ℃ and 28.6 ℃, respectively. While at the bottom surface, the temperature gradient was about 3 ℃ for both cases.

6. COMPARISON WITH AASHTO'S GRADIENT MODEL

Figure 10 shows the comparison between the predicted distribution of the maximum positive temperature gradient, which is discussed in the previous section and the design temperature gradient of Zone 1 of the AASHTO specification. Figure 10(a) shows the comparison along the full depth of the box-girder, in which it is clear that there is a good agreement with the AASHTO's gradient. For better visualization and ease, only the top 2 m and the bottom 1 m of the girder were drawn against the AASHTO's gradient in Figure 10(b). This is because as discussed in the previous

section, the real variation occurred with these two regions, while the temperature was almost constant along the clear depth of the web. As shown in Figure 10(b), the maximum gradients at the top surface are almost identical, where the predicted maximum temperature gradient was 29.6 ℃ , while the AASHTO's maximum temperature gradient is 30 ℃. At the bottom region of the girder, the behaviors and the gradient values are also very close. The predicted gradient is almost linear along the bottom 0.2 m of the girder with a maximum gradient less than 3 ℃, which is almost identical with the linear variation of the AASHTO along this region and with the gradient of the AASHTO at the bottom surface, which equals 2.8 ℃.

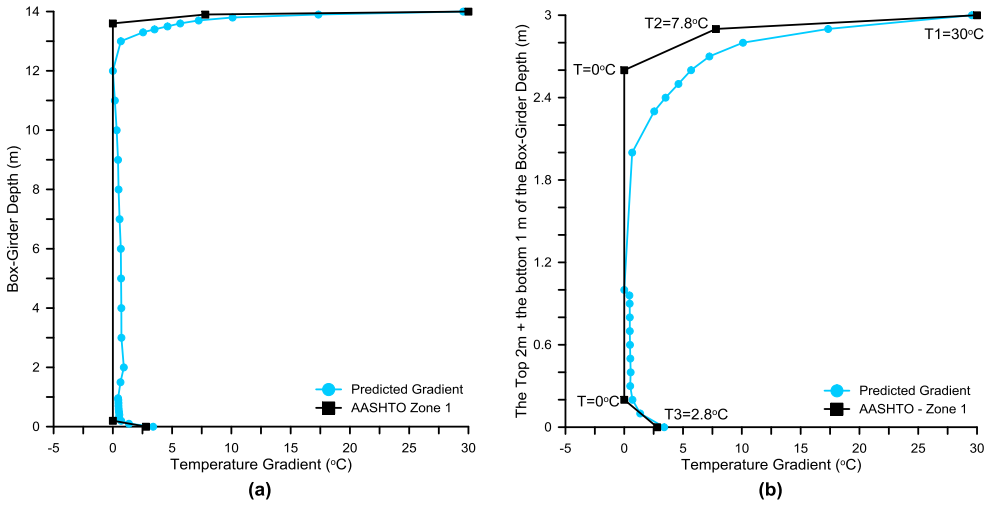

Figure 10 Comparison of the predicted maximum vertical temperature gradient with the gradient of the AASHTO (Zone1): (a) along the depth of the box-girder and (b) along the top 2 m plus the bottom 1 m

The main difference between the two gradients is the behavior along the top region (almost the top 1 m). The AASHTO gradient is bilinear with 7.8 ℃ at 0.1 m from the top surface and reaching its zero value (constant temperature region) at 0.4 m below. On the other hand, the predicted gradient distribution shows a nonlinear variation along this region with much higher temperature gradients at these two points. The predicted temperature gradients at 0.1 and 0.4 m were 17.3 ℃ and 5.7 ℃, respectively. Another important notice is that the predicted maximum temperature gradient was calculated for recorded weather data; hence, it is inadequate for extreme weather conditions. Considering extreme air temperature variation and solar radiation intensity with long return period as worked by all design codes, the gradient would be higher and hence the current AASHTO gradient would not be satisfactory for the case of deep box-girders in the region of Gaziantep, Turkey.

7. COCLUSIONS

The heat conduction and the temperature distributions in deep concrete box-girder bridges were studied in this research using the finite element method. External thermal loads including solar radiation, reflected radiation fluxes, surface convection cooling and surface re-radiation were considered in the thermal analysis. The finite element model was verified with climate data and temperature measurements from an existing bridge and was used to study the temperature and the temperature gradient distributions in deep box-girder sections for the summer weather conditions of Gaziantep in Turkey. Finally, the predicted maximum gradient was compared with the AASHTO provisions. The main conclusions of the current study are:

1. The proposed finite element thermal analysis could simulate the heat budget of the real box-girder and predict concrete temperatures with high accuracy. The AAE between the predicted and the measured concrete temperatures along different sections were in the range of 0.1℃ to 1.1 ℃, while the MAE was less than 1.7 ℃.
2. During the day, the temperature of the exterior surfaces increase due to the high solar radiation and the hot air, while because of the weak thermal conductivity of concrete, the concrete interiors still cold which results in a positive temperature gradient with a maximum at the exterior surface. On the other hand, due to the convection cooling and the surface re-radiation, a negative temperature gradient occurs at the early morning hours with a minimum temperature at the exterior surface. The predicted maximum positive temperature gradients across the thickness of the mid-lengths of the top slab, the bottom slab, the south web and the north web for the summer case in Gaziantep were approximately 25 ℃, 6 ℃, 7 ℃ and 11 ℃, respectively.
3. Due to the movement fashion of the sun during June, the maximum lateral temperature gradients occur at the southern surfaces, while lower thermal gradients occur at the northern surfaces of both the top and the bottom slabs. Along the centerline of the top slab, the predicted maximum positive temperature gradients at the southern and northern edges were approximately 9 ℃ and 3 ℃. On the other hand, the maximum positive gradients at the southern and northern edges for the centerline of the bottom slab were approximately 11 ℃ and 7 ℃.
4. For summer conditions of Gaziantep, the distribution of the maximum temperature gradient along the 14 m depth of the deep box-girder can be categorized into three different regions. The first region is a sharp nonlinear temperature decrease within the top 1 m. Followed by a region of a semi-constant temperature along the clear depth of the web in addition to the top depth of the bottom slab, ending with the third region which extends along the lower 0.2 m of the bottom slab, within which the temperature gradient shows a limited semi-linear increase down to the bottom surface.
5. The comparison of the predicted maximum vertical temperature gradient with the AASHTO's design gradient of zone 1 shows that the predicted gradient meets well the AASHTO's proposed temperature gradients at the top and the bottom surfaces. The design gradients of zone 1 at the top and the bottom surfaces are 30 ℃ and 2.8 ℃, while the predicted gradients at the same surfaces at the time of maximum gradient were 29.6 ℃ and 3.4 ℃. However, the gradient distribution behavior along the top 1 m is different. AASHTO suggests a bilinear gradient distribution along the top 0.4 m only, while the predicted gradient seems to vary nonlinearly within the top 1 m.

REFERENCES

[1] White I.G. Nonlinear temperature differential distributions in concrete bridge sructures: a review of the current literature, Technical Report 525, Cement and Concrete Association, USA, 1979.

[2] Zichner T. Thermal effects on concrete bridges, CEB Enlarged Meeting-Commission 2-Piva, 1981, pp. 292-313.

[3] Elbadry M., Ghali A. Thermal stresses and cracking of concrete bridges, *ACI Journal*, **83**(6), 1986, pp. 1001-1009.

[4] Massicotte B., Picard A., Gaumond Y., Ouellet C. Strengthening of long span prestressed segmental box girder bridge, *PCI Journal*, **39**(3), 1994, pp. 52-65.

[5] Lee J-H. Behavior of precast prestressed poncrete bridge girders involving thermal effects and initial imperfections during construction, *Engineering Structures*, 2012, **42**, pp. 1-8.

[6] Zhou G.D., Yi T.H. Thermal loads in large-scale bridges: a state-of-the-art review, *International Journal of Distributed Sensor Networks*, **2013**, 2013, pp. 1-17.

[7] Priestly M.J.N. Design thermal gradients for concrete bridges, *New Zealand Engineering*, **31**(9), 1976 213-219.

[8] Emerson M. Bridge temperatures for setting bearing and expansion joints, TRRL Supplementary Report 479, Transport and Road Research Laboratory, Berkshire, UK, 1979.

[9] Imbsen R.A., Vandershaf D.E., Schamber R.A., Nutt R.V. Thermal effects in concrete bridge superstructures, National Cooperative Highway Research Program Report 276, Transportation Research Board, Washington, DC, USA, 1985.

[10] AASHTO. AASHTO LRFD Bridge Design Specifications, American Association of State Highway and Transportation Officials, 2012, Washington DC, USA.

[11] Ghali A., Favre R. and Elbadry M. Concrete Structures: Stresses and Deformation. Spon Press: London, UK, 2002.

[12] COMSOL Multiphysics v 4.3a. Heat Transfer Module User's Guide, Stockholm, Sweden, 2012.

[13] Sveinson T.N. Temperature Effects in Concrete Box Girder Bridges, PhD Thesis, University of Calgary, Canada, 2004.

[14] Tayşi, N. and Abid, S. R. Temperature distributions and variations in concrete box-girder bridges: experimental and finite element parametric studies. *Advances in Structural Engineering*, **18**(4), 2015, pp. 469-486.

[15] Abid, S. R., Tayşi, N. and M. Özakça. Three-dimensional thermal modeling of temperature variation in concrete box-girders using COMSOL®, in: Proceedings of the 2014 COMSOL Conference in Cambridge, Cambridge, UK, 2014.

[16] Abid, S. R., Alhatmey, I., Tayşi, N. and M. Özakça. Finite element analysis of temperature distributions in precast concrete girders subjected to thermal loads. in: Proceedings of the 11th International Congress on Advances in Civil Engineering ACE, Istanbul, Turkey, 2014.

[17] Abid, S. R., Tayşi, N. and M. Özakça. Experimental analysis of temperature gradients in concrete box girders. *Construction and Building Materials*, **106**, 2016, pp. 523-532.